DOI: 10.53375/ijecer.2024.406

Transmission Coefficient Measurements using a 2.48-4.7 GHz Lateral Multiband Microstrip Patch Antenna (MB-MPA)

Koyu Chinen[1*], Shoko Nakamono[2], Ichiko Kinjo[3]
[1,2]GLEX, Japan,
[1]*Email: koyu.chinen@nifty.com*, [2]*Email: sk@glexworld.com,*
[3]National Institute of Technology, Okinawa College, Japan,
Email: ichi@okinawa-ct.ac.jp
[*] *Corresponding author*

Abstract: **We designed a standard triple-wavelength multiband microstrip patch antenna (MB-MPA) by electromagnetic simulation and fabricated it using an FR-4 substrate. The fundamental resonant frequency f_1 was 2.48 GHz, the second-order resonant frequency f_2 was 3.7 GHz, and the third-order resonant frequency f_3 was 4.7 GHz. The f_2 signal resonated at 1/2 the length of the patch width W, and the electrical field intensities of E_φ and E_θ showed $\pi/2$ rotation polarization relative to the f_1 signal. The polarization angle of the f_3 signal was about 34 degrees as the f_3 signal resonated at a length of 1/2 of the oblique line of the right triangle consisting of the shortened length L and 1/2 of the width W of the patch. The 0.1 - 6 GHz frequency band reflection and transmission coefficients of S-parameters S_{11} and S_{21} measured at a spatial propagation distance of 0.1 - 0.3 m with MB-MPAs as the transmitting and receiving antenna were consistent with the transmission system simulation results. The simulated transmission coefficient S_{21} at three wavelengths with a spatial propagation distance of 10 - 50 m with two-stage LNAs showed practical values. The lateral resonant MB-MPA can be practically designed by using 3D electromagnetic current density distribution, electric field intensity radiation, and evaluating the transmission coefficient S21.**

Keywords: **MB-MPA, muti-band microstrip patch antenna, transmission coefficient S_{21}, 3D electrical field radiation intensity pattern**

I. INTRODUCTION

The microstrip antenna (MPA) is a planar antenna consisting of a metal film as a radiation element (patch) on the front surface of a dielectric substrate coated with a metal conductor ground on the backside. The MPAs are used for wireless communications in the S-band (2-4 GHz), C-band (4 - 8 GHz), and X-band (8-12 GHz) frequency bands because of their ease of design and fabrication. For example, there are reports of MPAs in the 2.5 GHz band [1] using FR-4 substrate ($\varepsilon_r = 4.3$) and in the 3.5 GHz band [2] using low-k substrate ($\varepsilon_r = 2.2$) with a standard rectangular patch as the radiating element. The MPA has a narrow resonant frequency bandwidth because it utilizes the resonance phenomenon of the dielectric sandwiched between the frontside patch and the backside ground metals. Therefore, studies of 5.5 GHz band MPA using multiple high dielectric constant superstrates to increase the gain [3] and 5.28 GHz band MPA [4] have attempted to broaden the frequency bandwidth by forming slots in the patch. In addition, studies of multiband microstrip patch antennas (MB-MPAs) for multi-band applications for Wireless Fidelity (Wi-Fi, 2.4, 5, 6, 7.25 GHz), Long Term Evolution (LTE, 4G, 1.92-2.17 GHz), and the fifth-generation mobile communication system (5G, 1.7-4.5 GHz) wireless communication applications are being actively conducted. For example, 2.5 and 3.5 GHz MB-MPAs [5], 2.354 and 2.451 GHz MB-MPAs [6], 3.45 and 5.9 GHz MB-MPAs [7], 2.4-2.73 and 3.4-5.73 GHz MB-MPAs [8] as dual frequency MB-MPA, 2.4, 3.7 and 4.7 GHz MB-MPAs [9], 2.45, 3.5 and 4.65 GHz MB-MPAs [10], as triple frequency MB-MPA, 7.2-19.3 GHz MB-MPAs [11] as quadruple frequency MB-MPA and 5-12 GHz MB-MPAs [12] as quintuple frequency MB-MPA. A single-wavelength but high-frequency-specific antenna was designed as a 10 GHz MPA [13]. There are also studies on circular-slot 2 and 11 GHz MB-MPAs [14], hexagonal-slot 8.5 GHz MB-MPA [15], and circular-patch 2.45 GHz MB-MPA [16] with different slot and patch surface geometries, and a combined antenna MPA with broaden bandwidth Inverted-F antenna (IFA) 4.83–6.1 GHz [17] were studied. Furthermore, there are reports of 10 GHz 2 x 4 elements [18] and 3.5 GHz 4 x 4 elements [19] array antennas with multiple MPAs.

In these studies, new design proposals are mainly based on evaluating S-parameter reflection coefficients S_{11} using electromagnetic simulations, and there are few measurements of the transmission coefficients S_{21} of proposed antennas. We have designed and fabricated a standard rectangular-patch triple-wavelength MB-MPA, measured the reflection coefficient S_{11} and transmission coefficient S_{21}, and analyzed the current density distribution on the patch surface and the 3D (three-dimensional) electric field intensity radiation distribution using electromagnetic field simulation to clarify the signal resonance mechanism of multiple wavelengths, conducted transmission experiments using a vector network analyzer (VNA), transmitter and receiver MB-MPAs, and low-noise amplifier (LNA) to confirm the signal communication using the multi-band frequencies, and investigated the possibility of long-distance communication (10 to 50 m) through transmission and reception experiments using the VNA, MB-MPA, and two-stage LNA, and transmission system simulations.

II. 2.48-4.7 GHz MULTIBAND MICROSTRIP PATCH ANTENNA (MB-MPA)

We used electromagnetic simulators (AXIEM, EM Sight) [20] and Sonnet Lite [21] to analyze the frequency response of the S-parameter S_{11} in the design of a multiband microstrip patch antenna (MB-MPA). Several simulators were used to compare the validity of the S-parameter S_{11} values, and all simulators yielded nearly identical values. Figure 1 shows a dimensional drawing and a photograph of the fabricated MB-MPA. A glass-epoxy composite substrate was used as the antenna substrate (FR-4, t = 1.6 mm, ε_r = 4.6, 60 × 60 mm) with 35 µm-thick copper film on both sides. A 50 Ω microstrip line (MSL) with a width of 3 mm was used to feed the MB-MPA, and a board-terminal-mounted sub-miniature A-type (SMA) connector was used to connect the MB-MPA to the coaxial cable between the MSL and the signal source. Since the MB-MPA is a resonator, its resonant frequency is sensitive to the relative permittivity ε_r of the substrate (FR-4), making it applicable to aqueous solution sensors (1.8 - 7.3 GHz) [22]. Therefore, controlling the relative permittivity ε_r in the design and fabrication of MB-MPA with narrow resonance frequency bandwidths is essential.

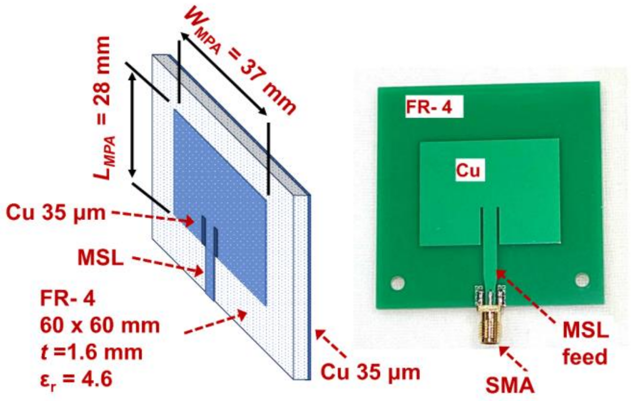

Fig. 1. Dimensional drawing and a photograph of the fabricated 2.48-4.7 GHz multiband microstrip patch antenna (MB-MPA) fabricated on FR-4 substrate.

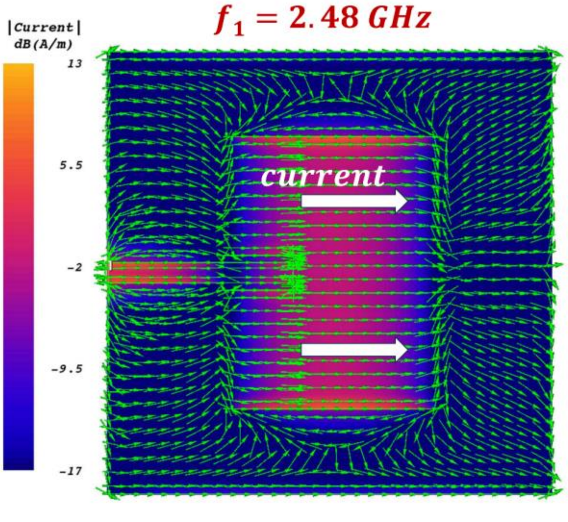

Fig. 2. The current density distribution at the fundamental resonant frequency (f_1 = 2.8 GHz) on the patch surface of 2.48-4.7 GHz MB-MPA analyzed by electromagnetic field simulation.

III. CURRENT DENSITY DISTRIBUTIONS AND 3D ELECTRIC FIELD RADIATIVE INTENSITIES OF MB-MPA

The current density distributions at the patch antenna surface for three multi-band frequencies of 2.48, 3.7, and 4.7 GHz were analyzed by electromagnetic field simulation.

The current density distribution at the fundamental frequency f_1 = 2.48 GHz is shown in Fig. 2, indicating that the current supplied from the feed line of the MSL resonates at a frequency that is approximately λ/2 the length of the LPA of the MPA.

Figure 3 shows the current density distribution at the patch antenna surface at the second-order resonant frequency (f_2 = 3.7 GHz). The second-order resonant resonance occurs at approximately one-half of the patch antenna's width (W_{PA}) in the direction of π/2 rotation of the current direction of the current density distribution at the fundamental frequency (f_1 = 2.48 GHz).

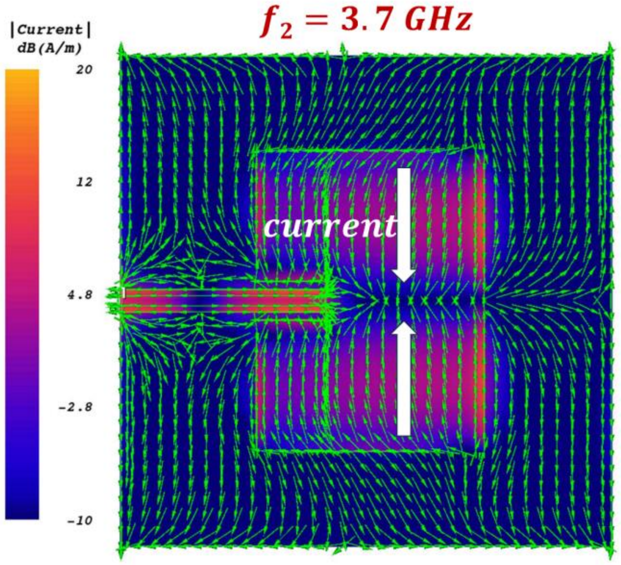

Fig. 3. The current density distribution at the second resonant frequency (f_2 = 3.7 GHz) on the patch surface of 2.48-4.7 GHz MB-MPA analyzed by electromagnetic field simulation.

Figure 4 shows the current density distribution at the patch antenna surface at the third-order resonant frequency (f_3 = 4.7 GHz). The current distributions have three parts, each a fan shape with a radius of $W_{MPA}/2$ and two corner shapes. The resonant frequency is determined by the $W_{MPA}/2$ and shortened L_{MPA}. The primary resonance occurs at the half-length of the oblique line of the shortened L_{MPA} and $W_{MPA}/2$ triangle, approximately 34 degrees rotated from the direction of the fundamental frequency f_1 = 2.48 GHz. The resonant current length distribution broadens the bandwidth of the resonant frequency f_3 compared to f_1 and f_2.

Assuming that the second-order and the third-order resonant frequencies are the fundamental frequencies at the resonant length L_{MPA}, plotting the relationship between the resonance frequency and the resonance length considering the L_{MPA} and the current density distribution of the patch antenna yields the graph in Fig. 5, and a formula f (GHz) = 70.72 / L_{MPA}-0.046 is obtained.

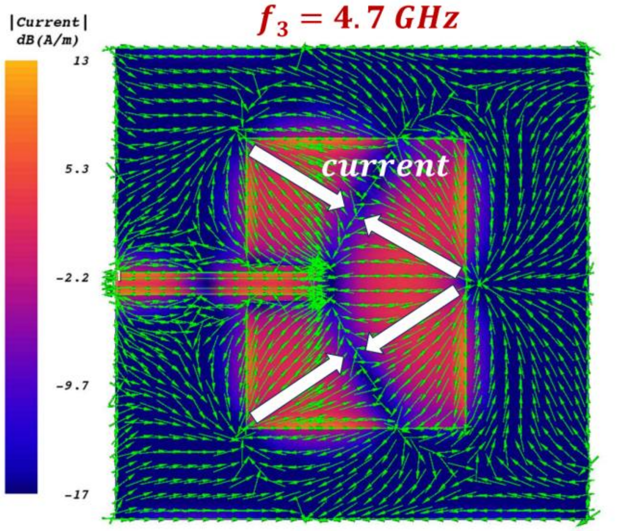

Fig. 4. The current density distribution at the third resonant frequency (f_3 = 4.7 GHz) on the patch surface of 2.48-4.7 GHz MB-MPA analyzed by electromagnetic field simulation.

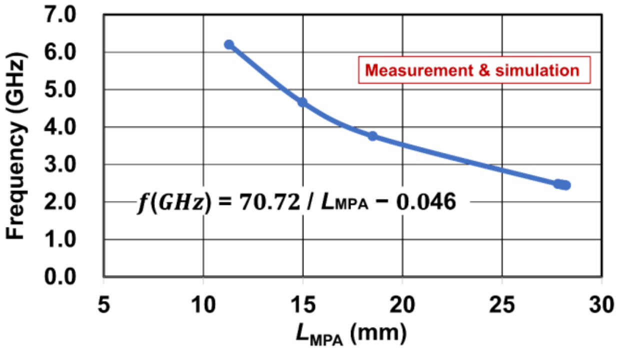

Fig. 5. Simulated and measured values of the resonant frequencies when the L_{MPA} of the MPA was varied.

Considering the resonant surface of a rectangular patch of length L_{MPA} and width W_{MPA}, a rectangular resonance model can be applied for the first- and second-order resonances from the current density distribution of the MB-MPA, and the resonant frequency f_{mn} can be obtained by the following equation (1), which is derived from the cutoff resonant condition of $(\omega/C)^2 = k_m^2 + k_n^2$, where C is the light velocity ($\approx 3 \times 10^8$ m/s), k_{mn} is the wavenumber, ε_r (4.6) is the relative permittivity of the substrate, the effective resonant lengths of the substrate L_{MPAe} and W_{MPAe} are 28.2 mm and 37.8 mm, respectively, and the resonance mode orders m and n are integers.

$$f_{mn} = \frac{C}{2\sqrt{\varepsilon_r}} \sqrt{\left(\frac{m}{L_{MPAe}}\right)^2 + \left(\frac{n}{W_{MPAe}}\right)^2} \tag{1}$$

Since the first-order resonance occurs at m =1 and n = 0, as shown in Fig. 2, the first-order frequency f_{10} = 2.48 GHz is calculated using (1). Since the second-order resonance occurs at m = 0 and n = 2, as shown in Fig. 3, the second-order frequency f_{02} = 3.7 GHz is calculated using (1). The third-order resonant frequency is considered equivalent to the resonance of the oblique line of a right-angle triangle with a shortened L_{MPAe} (24.1 mm) and a $W_{MPAe}/2$ (18.9 mm), from the MB-MPA's current density distribution, as shown in Fig. 4. The third-order frequency f_{12} = 4.7 GHz and the resonant wavelength 14.87 mm of the 1/2 oblique line are calculated using (1). The resonant wavelength of 14.87 mm at 4.7GHz coincides with the graph plotted in Fig. 5.

We can obtain the electric field intensity radiated from the current density flowing through a small segment of the patch antenna using Maxwell's electromagnetic field equations. The θ-directional component E_θ and φ-directional component E_φ of the magnitude of the electric field intensity radiated from the current element of length l and the current density i at the center of the x-y-z coordinates shown in Fig. 6 over a distance of r can be expressed by equations (2) and (3), respectively, where, the wavenumber is $k = 2\pi/\lambda$. The equations (2) and (3) are expressed at $\varphi = 0$ and $\theta = 90°$, respectively, to simplify the understanding. The fundamental difference between E_θ and E_φ is the variable angular coefficients of $\cos\theta$ and $\sin\varphi$.

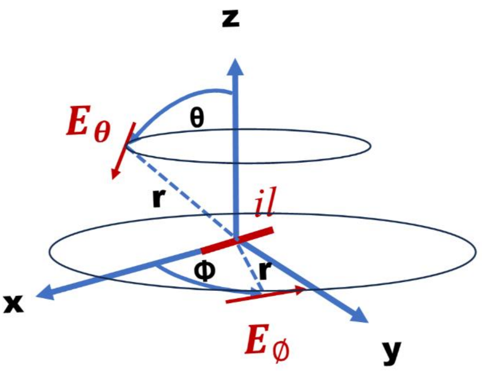

Fig. 6. The θ-directional component E_θ and φ-directional component E_φ of the magnitude of the electric field intensities radiated from the current element of the length l and the current density i at the center of the x-y-z coordinates.

$$E_\theta|_{\emptyset=0^\circ} = \frac{ile^{-jkr}}{j4\pi\omega\varepsilon_0}\left(\frac{1}{r^3} + \frac{jk}{r^2} - \frac{k^2}{r}\right)\cos\theta \tag{2}$$

$$E_\emptyset|_{\theta=90^\circ} = \frac{ile^{-jkr}}{j4\pi\omega\varepsilon_0}\left(\frac{1}{r^3} + \frac{jk}{r^2} - \frac{k^2}{r}\right)\sin\emptyset \tag{3}$$

We used an electromagnetic field simulator (AXIEM) [20] to obtain 3D electric field radiative intensities of E_θ and E_φ at each resonant frequency. The simulated intensity distributions of $E_{\theta1}$ and $E_{\varphi1}$ at the fundamental resonant frequency f_1 = 2.48 GHz are shown in Fig. 7. By using

Maxwell's theory of electromagnetism, the 3D electric field radiative intensities of $E_{\theta1}$ and $E_{\varphi1}$ are obtained by (2) and (3), respectively, reflecting the current magnitude and direction of the patch antenna surface. In this paper, however, $E_{\theta1}$ and $E_{\varphi1}$ denote magnitudes; the unit is dB rather than complex numbers.

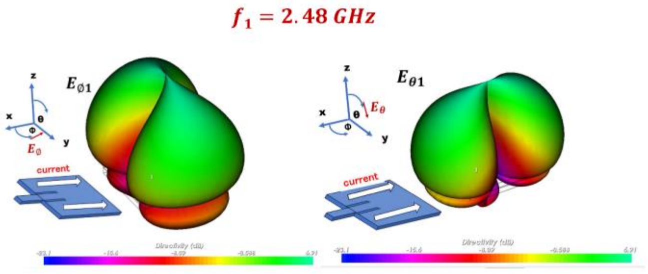

Fig. 7. The 3D electric field intensity distributions of $E_{\varphi1}$ and $E_{\theta1}$ at the fundamental resonant frequency f_1 = 2.48 GHz.

Figure 8 shows the 3D electric field intensity distributions of $E_{\theta2}$ and $E_{\varphi2}$ at the second-order resonant frequency f_2 = 3.7 GHz. This distribution shows the direction of the 3D electric field intensities of $E_{\theta1}$ and $E_{\varphi1}$ at the first-order resonant frequency f_1 = 2.48 GHz rotated by π/2.

As shown in Fig. 4, a part of the currents returns to the rear ground plane at the center of the patch, so the electric field radiation from the rear surface is relatively large.

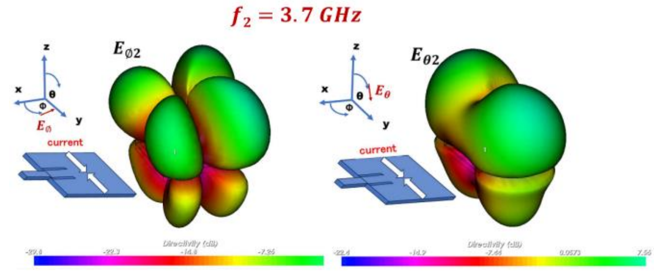

Fig. 8. The 3D electric field intensity distributions of $E_{\varphi2}$ and $E_{\theta2}$ at the second-order resonant frequency f_2 = 3.7 GHz.

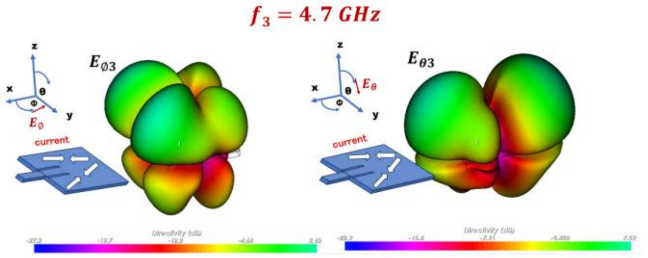

Fig. 9. The 3D electric field intensity distributions of $E_{\varphi3}$ and $E_{\theta3}$ at the third-order resonant frequency f_3 = 4.7 GHz.

Figure 9 shows the 3D electric field intensity distributions of $E_{\theta3}$ and $E_{\varphi3}$ at the third-order resonant frequency f_3 = 4.7 GHz. The directions of the 3D electric field intensities of $E_{\theta3}$ and $E_{\varphi3}$ are close to $E_{\theta1}$ and $E_{\varphi,}$ as the current direction at f_3 = 4.7 GHz on the patch antenna surface is approximately ±34 degrees to the current direction at f_1 = 2.48 GHz. On the other hand, the difference between the polarizations at f_2 = 3.7 GHz and f_3 = 4.7 GHz is significant. Since some of the currents returns to the rear ground plane at the center of the patch, as shown in Fig. 4, the electric field radiation from the rear surface is relatively large.

IV. TRANSMISSION COEFFICIENT S_{21} MEASUREMENTS WITH 2.48-4.7 GHZ MB-MPAS

The two MB-MPAs were used to measure the S-parameters reflection coefficient S_{11} and transmission coefficient S_{21} in the frequency range of 0.1 to 6 GHz using a vector network analyzer (VNA). The measured S-parameter results are shown in Fig.10. Hereafter, in this paper, the S-parameters S_{11} and S_{21} will be expressed in magnitude (dB) rather than complex numbers. The solid line is the measured value, and the dashed line is the simulated value. The spatial propagation distance d_s between the transmitting antenna (TxMPA) and the receiving antenna (RxMPA) were set to 0.1 m or 0.2 m, and the transmission coefficient S_{21} was measured using VNA. At the fundamental frequency f_1 = 4.8 GHz, the difference between the S_{21} values at the distance d_s = 0.1 m and 0.2 m was about 6 dB. This value is equivalent to the difference in the spatial propagation losses. Although the S_{21} values of higher-order mode frequencies are relatively low due to the multiple resonant directions, the fabricated MB-MPA can be applied to triple-frequency multiband wireless communications by adjusting the polarization and using an electrical amplifier. The fundamental frequency of f_1 = 2.48 GHz is used for WiFi in the 2.4 GHz band. The second-order resonant frequency of f_2 = 3.7 GHz and the third-order resonant frequency of f_3 = 4.7 GHz are used for LTE (4G), 5G, and local 5G communications, respectively.

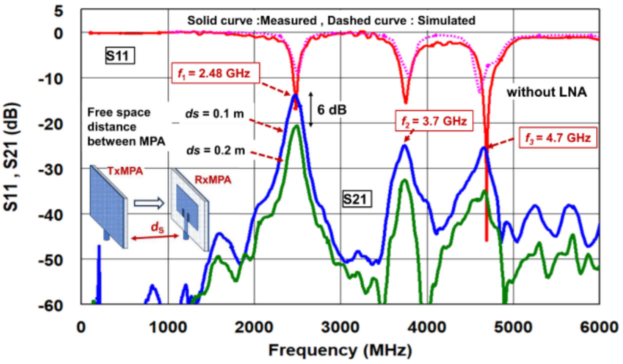

Fig. 10. The measured reflection coefficient S_{11} and the transmission coefficient S_{21} using 2.48-4.7 GHz multiband microstrip patch antennas (MB-MPAs) as a transmitting and receiving antenna (TxPMA and RxMPA) with a vector network analyzer (VNA). The frequency range is 0.1 to 6 GHz, and the spatial propagation distances d_s are 0.1 m and 0.2 m. The solid lines are measured values, and the dashed lines are simulated values.

We evaluated the transmission characteristic when the MB-MPA was rotated. When the receiving antenna RxMPA was rotated 90 degrees, related to the transmitting antenna TxMPA, the transmission coefficient S_{21} dropped by more than 10 dB. This is due to different polarization direction at each resonant frequency, as shown in Fig. 7, 8, and 9, even if the fundamental (f_1 = 2.48 GHz), second-order (f_2 = 3.7 GHz), and third-order (f_2 = 4.7 GHz) resonant frequencies are matched as shown in Fig. 11. When using MB-MPAs with the same resonant frequency, tilting, rotating the antenna to adjust the polarization direction is an effective way to suppress unwanted transmitted and received signals. The LNA is necessary to compensate for the decrease in the directional gain S_{21} for the higher-order resonant frequencies as the division of the lateral resonant currents degrades the S_{21}.

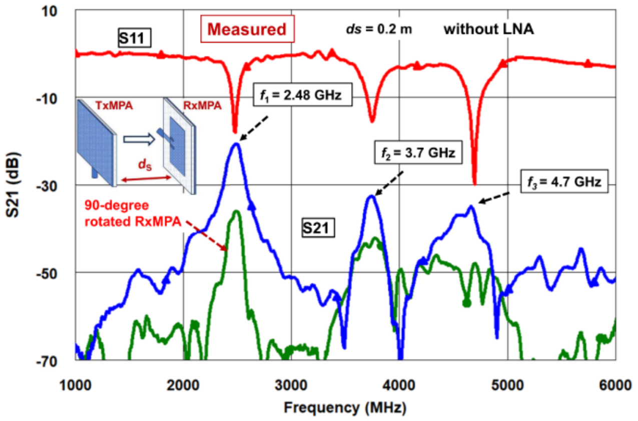

Fig. 11. Reflection coefficient S_{11} and transmission coefficient S_{21} were measured using a VNA and 2.48-4.7 GHz MB-MPAs with the receiving antenna RxMPA rotated 90 degrees relative to the transmitting antenna TxMPA. The propagation distance d_s is 0.2 m.

To investigate the transmission characteristics of the 2.48-4.7 GHz MB-MPA for longer propagation distance, an LNA was connected to the receiving antenna (RxMPA), and the transmission coefficient S_{21} was measured. The LNA was designed and fabricated using a SiGe bipolar junction transistor (BJT) with a transition frequency f_t = 80 GHz. The measured S_{21} in the frequency range from 0.1 to 6 GHz is shown in Fig. 12.

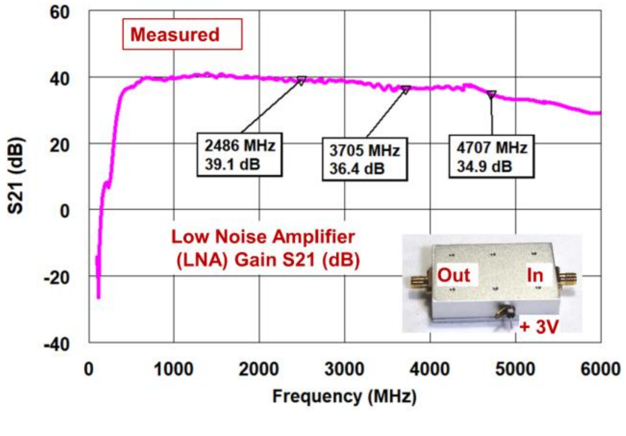

Fig. 12. The transmission coefficients S_{21} measured in the frequency range from 0.1 to 6 GHz of the LNA used in transmission experiments with the 2.48-4.7 GHz MB-MPA.

Transmission characteristics using a 2.48-4.7 GHz MB-MPA were analyzed using a visual system simulator (VSS) [20]. The transmission system configuration used for the transmission system simulation is shown in Fig.13, where the S_{21} characteristics of the MB-PA were calculated using the S_{11} measurements and a component block (PAS11) consisting of the S-parameter S_{21} file model. The transmitting and receiving antennas TxMPA and RxMPA are the built-in block models of the VSS. The spatial propagation distance d_s was incorporated into the built-in component parameters of the receiving antenna RxMPA.

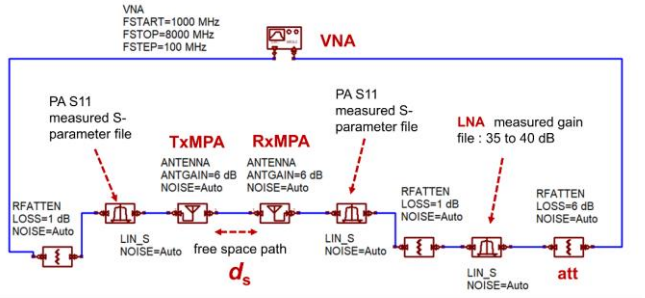

Fig. 13. Transmission system configuration for the system simulation using transmitting and receiving 2.48-4.7 GHz MB-MPAs. The PAS11 and the LNA component models are configured with the measured S-parameters.

The measured S_{21} values in the transmission using 2.48-4.7 GHz MB-MPAs with and without LNA for a spatial propagation distance d_s (0.3 m) and the results of the transmission system simulation are shown in Fig. 14. The measured (solid line) and simulated (dashed line) results of the S_{21} values without LNA show a slightly more significant difference at the third-order resonant frequency. Still, the measured and simulated values of S_{21} at the first- and second-order resonant frequencies almost overlap. When an LNA is connected to the RxMPA, the difference between the measured and simulated S_{21} values for the first-, second-, and third-order resonant frequencies is negligible. When the spatial distance ds is 0.3 m, a 6 dB attenuator suppresses the input signal power below the 1dB compression point (P1dB) at the VNA's input port, so the increase in the gain due to the LNA and the attenuator is about 34 dB at 2.48 GHz.

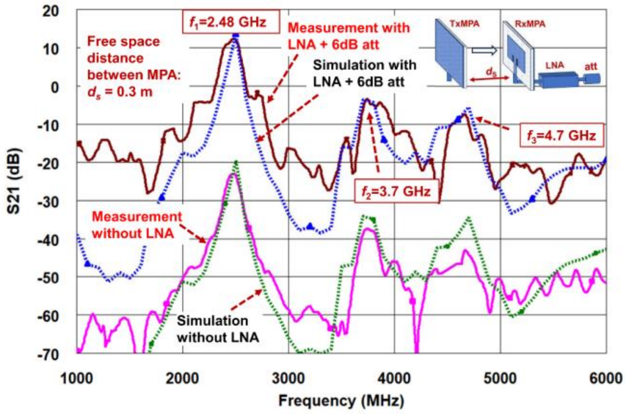

Fig. 14. Measured (solid line) and simulated (dashed line) results of the transmission coefficients S_{21} using the 2.48-4.7 GHz MB-MPAs. The spatial propagation distance d_s is 0.3 m. The lower curves in the graph show the results measured without LNA connected at the receiving antenna RxMPA, and the upper curves show the measured results with LNA and 6 dB attenuator connected.

For spatial propagation distances of d_s = 10 m, 30 m, and 50 m, the amplifier was configured with two-stage LNAs without attenuators and evaluated only by system simulation. The simulation results are shown in Fig. 15. Since the received power higher than -70 dBm is considered to be a practical level for quadrature amplitude modulation orthogonal frequency-division multiplexing (QAM-OFDM) wireless communication systems such as WiFi [23], long-distance communication using the first-order (f_1 = 2.48 GHz), the second-order (f_2 = 3.7 GHz), and the third-order (f_3 = 4.7 GHz) resonant frequencies with the 2.48-4.7 GHz MB-MPAs is feasible.

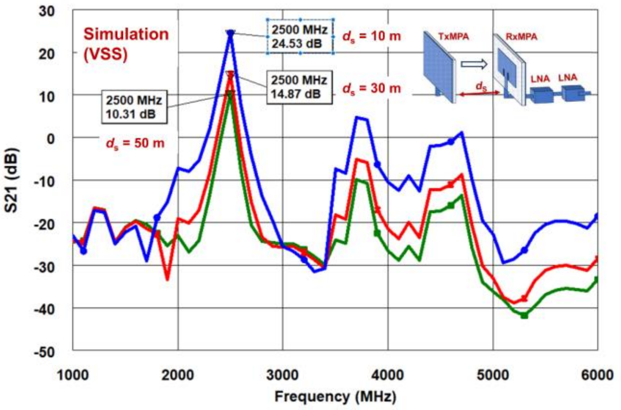

Fig. 15. System simulation results of long-range transmission characteristics using 2.48-4.7 GHz MB-MPAs. The spatial propagation distances d_s are 10, 30, and 50 m. Two-stage LNAs are connected to the receiving antenna RxMPA.

In the transmission of space propagating signals using 2.48-4.7 GHz MB-MPAs as transmitting antenna TxMPA and receiving antenna RxMPA, the 3D electric field strength distributions at first (f_1 = 2.48 GHz), second (f_2 = 3.7 GHz) and third (f_3 = 4.7 GHz) order resonant frequencies show that the polarization directions are 0, 90, and 34 degrees, respectively, as shown in Fig. 8, 9, and 10. Therefore, adjusting 0 degrees the rotation angle and tilt of the opposing transmitting antenna TxMPA's and receiving antenna RxMPA's is necessary. On the other hand, as an advantage, the signal interference from other antennas of different polarization can be significantly reduced by using the 2.48-4.7 GHz MB-MPAs as transmitting antenna TxMPA and receiving antenna RxMPA.

V. VALIDATION OF SYSTEM SIMULATION WITH FLISS TRANSMISSION FORMULA

We compared the system simulator (VSS) with the calculated values using Fliss' formula to validate it. The received signal power P_r can be obtained using equation (4), considering the transmitted signal power P_{in}, coaxial cable losses Γ_{CC1} and Γ_{CC2}, loss Γ_{S11} due to reflection coefficient S_{11}, transmission antenna directional gain G_{TxMPA}, spatial propagation loss Γ_{ds}, LNA gain G_{LNA1}, and G_{LNA2}. The spatial propagation loss Γ_{ds} is expressed as $(\lambda/(4\pi d_s))^2$.

$$P_r = P_{in}(\Gamma_{cc1} \cdot \Gamma_{S11} \cdot G_{TxMPA} \cdot \Gamma_{ds} \cdot G_{RxMPA} \cdot \Gamma_{S11} \cdot \Gamma_{cc2} \cdot G_{LNA1} \cdot G_{LNA2}) \tag{4}$$

$$\begin{aligned} S_{21}(dB) &= 10\log\frac{P_r}{P_{in}} \\ &= 10\log(0.79 \times 0.63 \times 3.98 \times 9.3 \times 10^{-7} \times 3.98 \times 0.63 \times 0.79 \times 8912 \times 8912) \\ &= -1 - 2 + 6 - 60.3 + 6 - 2 - 1 + 39.5 + 39.5 = 24.66\ (dB) \end{aligned} \tag{5}$$

Calculating the transfer coefficient S_{21} (dB) at a frequency f_1 = 2.48 GHz and spatial propagation distance d_s = 10 m, Equation (5) shows a value of 24.66 dB, which is almost identical to the simulated value by VSS (see Fig. 15). The values of the parameters in equation (5) are listed in Table I.

TABLE I. VALUES OF THE PARAMERTERS IN EQUATION (5)

Symbol	Description	Value	Value (dB)
Γ_{CC1}	Loss in connectors and cable	0.79	-1
Γ_{S11}	Loss by reflection at PA	0.63	-2
G_{TxMPA}	Directional gain of transmitter PA	3.98	6 (dBi)
Γ_L	Free space propagation loss	9.3×10^{-7}	-60.3
d_S	Free space distance	10	10 (m)
Γ_{S11}	Loss by reflection at PA	0.63	-2
G_{RxMPA}	Directional gain of transmitter PA	3.98	6 (dBi)
G_{LNA}	Gain of LNA	8912	39.5
Γ_{CC2}	Loss in connectors and cable	0.79	-1
f_C	Carrier frequency	2.48	2.48 (GHz)

VI. CONCLUSIONS

We designed an MB-MPA using an electromagnetic simulator for three resonant frequencies of f_1 = 2.48 GHz, f_2 = 3.7 GHz, and f_3 = 4.7 GHz, and fabricated it on an FR-4 substrate. The S-parameters S_{11} and S_{21} were measured using a VNA in the frequency range from 0.1 to 0.6 GHz. The measured results were in close agreement with the simulation.

The simulation of the current density distribution on the patch surface showed that the current at the frequency of f_2 = 3.7 GHz resonates in the direction of $\pi/2$ rotation to the current at the frequency of f_1 = 2.48 GHz on a plane that divides the patch width W_{PA} into two parts. The current at the frequency f_3 = 4.7 GHz resonates at about one-half of the oblique line of a right triangle with $W_{PA}/2$ and a shortened L_{PA}.

The 3D electric field intensity radiative patterns (E_θ and E_φ) reflected the current density distribution on the patch surface. The electric field intensities $E_{\theta 2}$ and $E_{\varphi 2}$ are $\pi/2$ rotated from $E_{\theta 1}$ and $E_{\varphi 1}$. The electric field intensities $E_{\theta 3}$ and $E_{\varphi 3}$ are about 34 degrees rotated from $E_{\theta 1}$ and $E_{\varphi 1}$.

The transmission coefficient S_{21} was measured using MB-MPAs as the transmitting and receiving antennas at spatial propagation distances d_s of 0.1, 0.2, and 0.3 m. The values of S_{21} decreased by about 10 dB when the transmitting antenna was rotated by $\pi/2$ to the receiving antenna. Signal communication using MB-MPAs requires matching the resonant frequency and the polarization direction. Therefore, the influence of interfering signals can be significantly reduced by shifting either the resonant frequency or the polarization direction from the interfering signal.

The measured and simulated values of S_{21} were almost consistent when the LNA was connected to the receiving antenna RxMPA, and the spatial propagation distance d_s was 0.3 m. In the transmission system configuration with two-stage LNA and the spatial propagation distances d_s of 10, 30, and 50 m, the simulation results provide insight into the possibility of long-distance communication at triple resonant frequencies of the MB-MPA.

The value of W_{MPA} significantly affects the higher resonant frequencies. In the design of lateral resonant MB-MPAs, it is necessary to simulate the design using 3D electric field intensity radiation and confirm the transmission characteristics by S_{21} measurement.

REFERENCES

[1] S. Rana, K. Sen, T. Mamun, S. Mahmud, M. Rahman, “A 2.45 GHz microstrip patch antenna design, simulation, and analysis for wireless applications,” *Bulletin of Electrical Engineering and Informatics*, vol. 12, no. 4, August 2023, pp. 2173-2184, ISSN: 2302-9285, DOI:10.11591/eei. v12i4.4770

[2] S. Rana, H.O. Rasid, S. K. S. Shuva, S. Ahmed, S. R. Islam, M. Rahman, “Design, Simulation and Analysis of 3.5 GHz Microstrip Patch Antenna for Wireless Communication Systems,” *4th ICCCNT IEEE Conference,* 2023, DOI:10.1109/ICCCNT56998.2023.10307552

[3] N. Hussain, U. Azimov, M. Jeong, S. Rhee, S. W. Lee, and N. Kim, “A High-Gain Microstrip Patch Antenna Using Multiple Dielectric Superstrates for WLAN Applications,” *The Applied Computational Electromagnetics Society Journal (ACES)*, vol. 35, no. 2, pp. 87-193, 2020.

[4] Y. Wang and Y. Lu, “The Strip-Ground Rectangular Patch Antenna,” *Hindawi International Journal of Antennas and Propagation,* vol. 201no. 7, Article ID 5924157, 2017. DOI:10.1155/2017/5924157

[5] I. Ali, and R. Y. Chang, “Design of Dual-Band Microstrip Patch Antenna with Defected Ground Plane for Modern Wireless Applications,” *2015 IEEE 82nd Vehicular Technology Conference (VTC2015-Fall)*, 2015. DOI:10.1109/VTCFall.2015.7390887

[6] H. Nornikman, B. H. Ahmad, M. Z. A. Abd Aziz, H. A. Bakar, “Dual Frequencies Band and Enhanced Wideband Effect of Dual Layer Microstrip Patch Antenna with Parasitic,” *IOP Conf. Series: Journal of Physics: Conf. Series,* 1049, 012012, 2018. DOI:10.1088/1742-6596/1049/1/012012

[7] S. K. Noor, M. Jusoh, T. Sabapathy, A.H. Rambe, H. Vettikalladi, A. M. Albishi, Himdi, “A Patch Antenna with Enhanced Gain and Bandwidth for Sub-6 GHz and Sub-7 GHz 5G Wireless Applications,” *Electronics,* vol. 12, no. 12, 2555, 2023. DOI:10.3390/electronics12122555

[8] M. Bikrat, S. Bri, A. G Bravo, A. M. Manterola, M. Gonzalez-Atienza, F. A. Amador, “Multi-Bandwidth Reconfigurable Patch Antenna for Devices in WLAN and UWB Technology Applications,” *Applied Sciences,* vol. 13, no. 16, 9367, 2023. DOI:10.3390/ app13169367

[9] O. Ossa-Molina, F. Lopez-Giraldo, “A Simple Model to Compute the Characteristic Parameters of a Slotted Rectangular Microstrip Patch Antenna,” *Electronics,* vol. 11, no. 1, 129, 2022. DOI:10.3390/electronics11010129

[10] Pragati, S.L. Tripathi, S. R. Patre, S. Singh and S.P. Singh, “Triple-band Microstrip Patch Antenna with Improved Gain,” *International Conference on Emerging Trends in Electrical, Electronics and Sustainable Energy Systems (ICETEESES–16),* pp. 106-110, 2016.

[11] M. A. Layegh, C. Ghobadi and J. Nourinia, “The Optimization Design of a Novel Slotted Microstrip Patch Antenna with Multi-Bands Using Adaptive Network-Based Fuzzy Inference System,” *Technologies*, vol. 5, no. 4, 75, 2017. 10. DOI:3390/technologies5040075

[12] Ahmad, G.O. Lee, D. y. Choi, “Design and Performance Evaluation of a Compact Frequency Reconfigurable Coplanar-Waveguide-Fed Slotted Patch Antenna for Multi-Band Wireless Communication,” *Electronics,* vol. 12, no. 18, 3889, 2023. DOI:10.3390/electronics12183889

[13] R. V. Gatti, R. Rossi, M. Dionigi, “Single-Layer Line-Fed Broadband Microstrip Patch Antenna on Thin Substrates,” *Electronics*, vol. 10, no. 1, 37, 2021. DOI:10.3390/ electronics10010037

[14] Y. Rhazi, O. E. Bakkali, Y. E. merabet, M. A. lafkih, S. Bri, M. N. Srifi, “Novel Design of Multiband Microstrip Patch Antenna for Wireless Communication,” *Advances in Science, Technology and Engineering Systems Journal,* vol. 4, no. 3, pp. 63-68, 2019. DOI:10.25046/aj040310

[15] M. Sharafeldin A. Boush, C. Kaur, “A Design for the Bandwidth Improvement for the Microstrip Patch Antenna for Wireless Network Sensor,” *International Journal of Scientific Research in Science, Engineering and Technology*, vol. 9, no. 3, pp. 396-403, 2022. DOI:10.32628/IJSRSET2293130

[16] N. Markad, S. Mahadik, “Broadband circular polarized patch antenna with harmonic suppression,” *Indian Journal of Science and Technology,* vol. 13, no. 38, pp. 4073-4083, 2020. DOI:10.17485/IJST/v13i38.1682

[17] X.-P. Li, Q.M. Zhang, L. Yan, C. Q. Wang, W. Li, “A Double-Layer Patch Antenna for 5–6 GHz Wireless Communication,” *Micromachines*, vol. 13, no. 6, 929, 2022. DOI:10.3390/ mi13060929

[18] L. C. Paul, I. Hasan, R. Azim, R. Islam, M. T. Islam, “Design of High Gain Microstrip Array Antenna and Beam Steering for X Band RADAR Application,” *Joint 9th International Conference on Informatics, Electronics & Vision (ICIEV) and 2020 4th International Conference on Imaging, Vision & Pattern Recognition (icIVPR)*, 2020. DOI:10.1109/ICIEVicIVPR48672.2020.9306519

[19] D.A. Jimenez, A. Reyna, L.I. Balderas, M.A. Panduro, “Design of 4×4 Low-Profile Antenna Array for CubeSat Applications,” *Micromachines*, vol. 14, no. 1, 180, 2023. DOI:10.3390/mi14010180

[20] https://www.cadence.com/en_US/home/tools/system-analysis/rf-microwave-design/awr-microwave-office.html

[21] https://www.sonnetsoftware.com/

[22] J. Yeo and J. Lee, “High-Sensitivity Slot-Loaded Microstrip Patch Antenna for Sensing Microliter-Volume Liquid Chemicals with High Relative Permittivity and High Loss Tangent,” *Sensor*, vol. 22, no. 24, 9748, 2022. DOI:10.3390/s22249748

[23] https://www.wi-fi.org/